Open Access

Journal of Energy and Power Technology

LIDSEN Publishing Inc.

Review

Hybrid Materials and Nanoparticles for Hybrid Silicon Solar Cells and Li-Ion Batteries

Antonio Vázquez-López [1], Marina García-Carrión [1], Erlend Hall [2], Anisa Yaseen [2], Ilknur Kalafat [3], María Taeño [1], Junjie Zhu [2], Xinyu Zhang [4], Elif Arici [5], Omer Suat Taskin [3], David Maestre [1], Emilio Nogales [1], Pedro Hidalgo [1], Julio Ramírez-Castellanos [6], Bianchi Méndez [1], Neslihan Yuca [3, 7], Smagul Karazhanov [2], Erik S. Marstein [2], Ana Cremades [1, *]

1. Department of Materials Physics, Physics Faculty, Complutense University of Madrid, Ciudad Universitaria, 28040 Madrid, Spain; E-Mails: antvaz01@ucm.es; margar02@ucm.es; m.taeno@ucm.es; dmaestre@ucm.es; enogales@ucm.es; phidalgo@ucm.es; bianchi@ucm.es; cremades@fis.ucm.es
2. Department for Solar Energy, Institute for Energy Technology, 2027 Kjeller, Norway; E-Mails: erlend.hall@outlook.com;anisa.yaseen@live.no; Junjie.Zhu@ife.no; Smagul.karazhanov@ife.no; Erik.Stensrud.Marstein@ife.no
3. Enwair Energy Technologies Corp., Sariyer, 34469 Istanbul, Turkey; E-Mails: kalafat@enwair.com; omersuat@enwair.com; nyuca@enwair.com
4. Zhejiang Jinko Solar Co. Ltd., No. 58 Yuanxi Road, Yuanhua Industrial Zone, Yuanhua Town, Haining, Zhejiang 314416, China; E-Mail: xinyu.zhang@jinkosolar.com
5. Energy Institute, Istanbul Technical University (ITU), Istanbul, Turkey; E-Mail: aricibogner@itu.edu.tr
6. Department of Inorganic Chemistry, Chemistry Faculty, Complutense University of Madrid, Ciudad Universitaria, 28040 Madrid, Spain; E-Mail: jrcastel@quim.ucm.es
7. Maltepe University, Marmara Eğitim Köyü, Maltepe, 34857 Istanbul, Turkey

* **Correspondence:** Ana Cremades; E-Mail: cremades@fis.ucm.es

Academic Editor: Zhao Yang Dong

Special Issue: Batteries: Past, Present and Future

Journal of Energy and Power Technology
2021, volume 3, issue 2
doi:10.21926/jept.2102020

Received: November 09, 2020
Accepted: April 17, 2021
Published: May 08,2021

Abstract

Hybrid composites based on inorganic nanomaterials embedded into a polymer matrix have were synthesized and characterized. Oxide semiconductor nanoparticles (SnO, SnO_2, TiO_2, Ga_2O_3, and NiO) and Si nanoparticles were employed as inorganic counterparts in the hybrid composite, while a conductive polymer (PEDOT:PSS) with diverse additives was used as the organic matrix. The composites were spin-coated on Si or glass substrates. The potential use of these materials in photovoltaic devices to improve Si surface passivation behavior was investigated. Besides, the use of the nanoparticles as active materials for anodes in Li-ion batteries was evaluated. Some other aspects, such as the durability and stability of these materials, were also assessed.

Keywords

Silicon; oxide nanoparticles; PEDOT:PSS; passivation; hybrid solar cells; Li-ion batteries

1. Introduction

Hybrid composites are materials composed of at least two compounds, mostly organic and inorganic, used to improve the properties of the parent material. Most commonly used organic compounds include carbon allotropies or polymers, while metallic and semiconducting nanomaterials have been usually used as the inorganic counterparts. These hybrid materials have recently emerged as good candidates in the fields of electronics, sensors [1, 2], photovoltaics [3], and other energy storage devices [4], mainly due to the positive synergy between organic and inorganic compounds and their low-cost and easy scalability. However, challenges are still being faced to improve these hybrid composites and widen their applicability in diverse fields of technological research.

Poly(3,4-ethylenedioxythiophene)polystyrene sulfonate (PEDOT:PSS) is a widely used conducting polymer with wide applications in energy storage devices [5], thermoelectrics [6], and photovoltaics [7], such as flexible solar cells, perovskite solar cells, and hybrid silicon solar cells [8-10], due to its unique properties including p-type behavior, optical transparency in the visible range, good electrical conductivity, chemical stability, and flexibility, thus allowing it to form different geometries as thin layers or films. However, it shows a relatively low conductivity, typically in the range of 0.1–1 S cm^{-1}, which is insufficient for a few applications. This behavior depends on the structure of PEDOT:PSS, which comprises two ionomers, PEDOT and PSS. PEDOT is water-insoluble, whereas PSS is water-soluble. PSS possesses a strong insulating behavior, which is directly related to the overall low conductivity of the polymers. Thus, controlling or modifying the ratio of PEDOT and PSS in the polymer or the Coulombic interaction is important to achieve enhanced electrical conductivity [11]. Further, its low stability at high temperatures, in UV light, and moisture should be overcome for its complete utilization.

Hybrid composites based on PEDOT:PSS in combination with inorganic nanomaterials have shown remarkable results so far [12]. The combination of inorganic and organic materials can provide improved stability and tunable electrical and optical properties and thus can be used for photovoltaics and energy storage devices. In this regard, PEDOT:PSS has shown great results as a

passivation layer for silicon [13] in different silicon-based solar cell architectures [14]. In order to push the boundaries and improve their performances, different approaches such as the addition of solvents [15-20] to control the SiO_x layer [10] and different post-treatments of the layers [21] have been established. Also, nanoparticle addition has shown some preliminary results of preventing PEDOT:PSS degradation since the addition of inorganic materials can enhance its performance [22]. In addition to the use of metallic nanostructures such as Ag or Au in the hybrid composites [21], the use of semiconductor nanomaterials as counterparts has garnered significant attention. Wide bandgap oxide semiconductors (WBS), such as SnO, NiO, SnO_2, TiO_2, and Ga_2O_3 nanostructures, have great optoelectronic properties due to high surface-volume ratio and low dimensions, making them a standpoint for solar cell or energy storage technologies. Further information on the synthesis and applications of these oxide nanomaterials can be found in the literature [23]. PEDOT:PSS has also been used as a binder in Li-ion battery anodes. The addition of Si nanoparticles [24] showed an improved specific capacity of the anode. Similarly, oxide nanoparticles have been used as high capacity anodes in Li-ion batteries [25-27], and their composites [28, 29] have demonstrated potential applicability in this field of research.

In this review, we present recent advances in hybrid/composite materials for energy-related applications. In particular, we focused on PEDOT:PSS and its functionalization with different nanoparticles, including Si and different oxide nanoparticles for the passivation of Si surface in photovoltaic devices and anode designing for Li-ion batteries.

2. Experimental Section

2.1 Metal Oxides and Silicon Nanomaterials

Among the different metal oxide nanoparticles, two p-type (SnO and NiO) and three n-type WBS (SnO_2, TiO_2, and Ga_2O_3) were selected. In recent years, various methods have been established to obtain highly crystalline nanoparticles with small average sizes. Different synthesis routes for oxide nanoparticles, including NiO [30], SnO_2 [31], TiO_2 [32], and Ga_2O_3 [33], summarized in Figure 1, can be followed to obtain the desired materials.

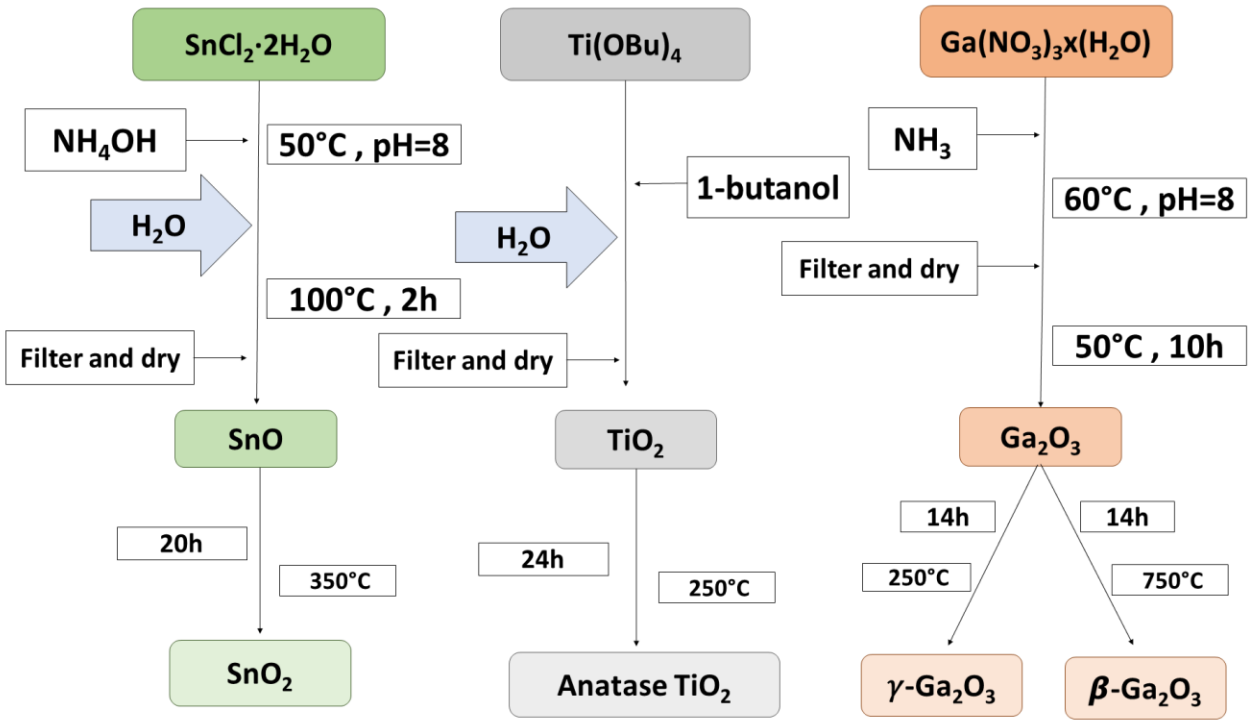

Figure 1 Chemical routes to synthesize SnO, SnO_2, anatase TiO_2, and Ga_2O_3 via hydrolysis.

SnO and SnO_2 nanoparticles were synthesized via chemical co-precipitation based on hydrolysis, as explained in [34] and [35], respectively. This method produced a large amount of highly crystalline nanoparticles fundamental for large-scale applications. Anatase TiO_2 synthesis [36] method was similar to that used for SnO_2 and followed a soft chemistry route based on hydrolysis to produce 5-8 nm-sized nanoparticles. Also, in the case of TiO_2, pH control of the reaction was not necessary, thus simplifying the synthesis route. Ga_2O_3 nanoparticles were obtained in two different phases, β and γ [37]. After the synthesis of the nanoparticles, as depicted in Figure 1, the obtained dry powder was heated for 14 h in a neutral atmosphere at two different temperatures, 750 °C to obtain β-Ga_2O_3 and 250 °C to obtain the γ-Ga_2O_3 nanoparticles. Nickel oxide (NiO) nanoparticles were synthesized following a hydrothermal procedure with optimized conditions as explained in [38] to ensure the production of highly crystalline nanoparticles.

The as-synthesized nanoparticles were further characterized by X-ray diffraction (XRD) (not shown here), transmission electron microscopy (TEM), and Raman spectroscopy (results not shown) to study their microstructure, morphology, size, and crystallinity [34-38]. The corresponding TEM images of TiO_2, SnO_2, and NiO nanoparticles are shown in Figure 2. The results showed that all the nanoparticles existed in a single phase with a size usually below 10 nm.

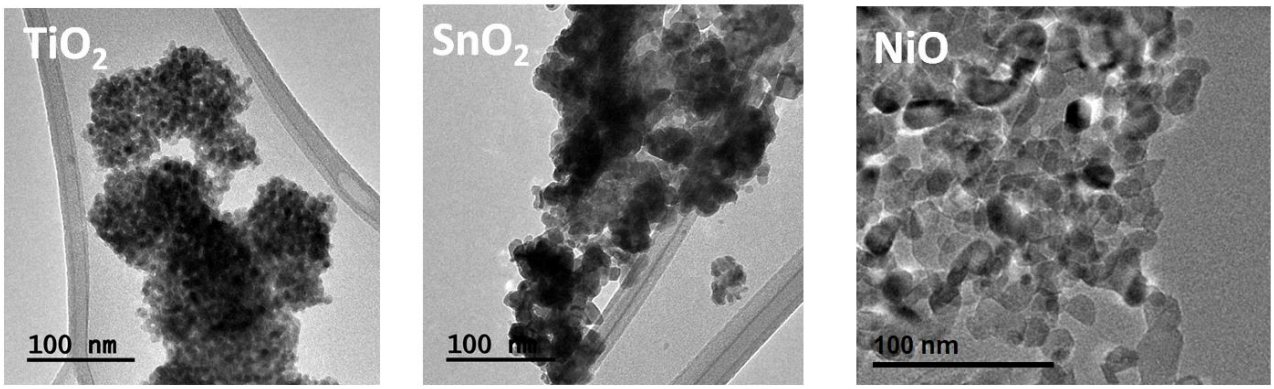

Figure 2 TEM images of the synthesized TiO_2, SnO_2, and NiO nanoparticles.

Si nanoparticles 30-50 nm in size were purchased from US-nano, whereas those of size 300 nm were provided by the Institute for Energy Technology (IFE, Norway).

2.2 Deposition of PEDOT:PSS Thin Films and Synthesis of Hybrid/Composite Films

Several efforts have been made to enhance the conductivity of PEDOT:PSS. Usually, post-treatment of the PEDOT:PSS layers with organic solvents such as dimethyl sulfoxide (DMSO) [15], ethylene glycol (EG), and diethylene glycol (DEG) have shown to improve the conductivity [21]. However, the addition of organic solvents in the PEDOT:PSS mixture before deposition, instead of treating the film with DMSO [16], EG [17], and other solvents [18], was chosen as the primary method to improve the conductivity of the polymer. Besides, surfactants like Triton X-100 [19] have shown remarkable improvement in the overall wettability and surface coverage, including conductivity. The polymer mixture was prepared by mixing PEDOT:PSS (Clevios, PH1000, 1.0%-1.3% wt. in water) and DMSO or EG (both 5% wt.) in different concentrations [20]. Triton X-100 was also added in 0.1% wt. and higher concentrations to assess its effect on the overall coating properties and achieve improved wettability and slightly increased conductivity.

In order to prepare a hybrid composite, a controlled amount of the selected inorganic nanoparticles were added to the PEDOT:PSS-based mixture and magnetically stirred for 2 h. Following this, the mixture was filtered with a polyethersulfone (PES) membrane (pore size = 0.45 μm) to achieve higher homogeneity. Furthermore, some other parameters were also evaluated in this work. The obtained PEDOT:PSS-based mixture or the composite with inorganic nanoparticles (either Si or metal oxides) was spin-coated on n-type or p-type silicon float-zone (FZ) substrates (TOPSIL, thickness 280.00 ±20 nm) as described in [34, 36, 37]. Glass substrates were also used when necessary and were pre-treated with isopropanol and boiling water and dried with N_2. Some other substrate post-treatments, such as thermal treatment to evaporate the remaining water or solvents, were also evaluated in this review.

2.3 Cell Preparation and Test Procedure

For the preparation and testing of the anodes using SnO_2, please refer to [35]. For TiO_2 and Si based-anodes active materials, binder and carbon black (CB) were mixed in water (weight ratio of TiO_2/(PAA)/CB = 70/20/10, Si/PA:PVA/CB/CNT = 70/20/7.5/2.5, and Si/PEDOT:PSS = 80/20) and stirred for 3 h. Slurries were coated on the surface of copper foil by a doctor blade. After drying, the

electrodes were cut as disks for coin cell assembling. They were placed in the glovebox overnight and further dried in a vacuum oven at 90 °C for 12 h to completely remove the water. Celgard 2400 separator obtained from Celgard PAA (Mw: 450,000, Sigma Aldrich) was used as the binder. Lithium-ion electrolyte (BASF), 1.2 M lithium hexafluorophosphate ($LiPF_6$) in ethylene carbonate (EC), diethyl carbonate (DEC) (EC/DEC = 3:7 by weight), and fluoroethylene carbonate (FEC, 30% by weight) were added together. The electrodes were used to assemble the coin cells. The Li metal was used as a counter electrode. The performance of the assembled 2032 coin cells was evaluated with the Neware battery test system. The cut-off voltage of cell testing was between 1.2 V and 0.01 V, assuming a theoretical value of 3500 mAh/g for Si and 330 mAh/g for TiO_2. Half cells were cycled at C/25 for 2 cycles, C/10 for 2 cycles, and C/5 for the following cycles.

2.4 Electrode Characterization

TEM images were acquired with a JEOL JEM 1400 TEM microscope, while Raman spectroscopy measurements were carried out on a confocal microscope Horiba Jobin Yvon LabRam HR 800 using a He-Ne red laser (λ = 633 nm) and a He-Cd UV laser (λ = 325 nm) equipped with a charge-coupled device (CCD). Different neutral filters were used to attenuate the total laser intensity by a factor of 0.5, 0.25, and 0.1. Hall effect measurements were performed at room temperature using a Hall Ecopia AMP55T HMS-7000 equipped with four gold probes. Gold contacts (20 nm thick) were deposited with thermal evaporation (Quorum Q150T ES) using a mask to obtain contacts with the Van der Pauw configuration. On top of the Au contacts, silver paint was deposited.

Optical absorption was measured with a UV-vis-NIR light source DH-200 ocean optics with a deuterium and halogen lamp. Effective charge carrier lifetime values were calculated from the PL intensity based on the quasi-steady-state photoconductance (QSS-PC) measurements using a LIS-R1 PL imaging setup from BT Imaging with an excitation wavelength of 808 nm and constant illumination intensity of 4.2×10^{-2} W cm^{-2}. Silver contacts were deposited with the aid of a mask by Kurt J Lesker FTC-2800 thermal evaporator. I-V curves were obtained with a Keithley 4200 semiconductor characterization system.

3. Results and Discussion

3.1 Hybrid Materials for Si Passivation and Solar Cells Applications

PEDOT:PSS/Si solar cell junctions have shown high power efficiency [14, 39], thus garnered interest as promising p-n junction materials for high-efficiency solar cells. However, PEDOT:PSS layers should fulfill different requirements, such as homogeneity in the deposition process, high mobility of charge carriers, and low degradation over time, to be used as a p-n junction. The inorganic/organic interface between silicon and PEDOT:PSS has been widely investigated to obtain long-lasting and high-performance solar cells.

Previous results have shown that the addition of a range of compounds could boost PEDOT:PSS conductivity. Among them, nanoparticles such as metallic Au and Ag have improved film properties due to the modified electrostatic interaction between PEDOT and PSS [40]. Recently, oxide nanoparticles such as TiO_2 and SnO_2 have been tested and some preliminary results were obtained [15], showing that inorganic WBS could lead to highly conductive PEDOT:PSS films. García-Tecedor et al. [22] reported that adding 0.5% wt. of SnO_2 to the PEDOT:PSS matrix, deposited over n-type

silicon, improved the passivation behavior as the carrier lifetime was increased by seven times; also, better I-V rectification behavior was shown. In addition, a simple spin-coating method for effective deposition of PEDOT:PSS was described.

Hence, firstly, PEDOT:PSS passivation of the floating zone (FZ) Si wafer was studied, including the inorganic nanoparticles in the hybrid material. Different wide bandgap semiconductor oxide nanoparticles were tested, including both n-type (SnO_2, TiO_2, Ga_2O_3) and p-type (SnO and NiO) oxide materials as well as silicon nanoparticles.

3.1.1 PEDOT:PSS/Silicon Interfaces

Good surface passivation was obtained by spin-coating PEDOT:PSS over FZ silicon [41], most noticeable when higher concentrations of Triton X-100 were used, which further improved the adhesion of PEDOT:PSS on the surface of the untreated Si. Moreover, HF-treated Si was used to assess the effect of etching on the native silicon layer, which also showed good adhesion and coverage. Stability over time was analyzed by measuring the carrier recombination, as observed in Figure 3, which displays the PL images of the films over 42 days. The results showed that the degradation of charge carrier lifetime was reduced to 260 µs within about three weeks and then stabilized at around 160 µs. In addition to low surface recombination velocities, good uniformity across large areas was obtained.

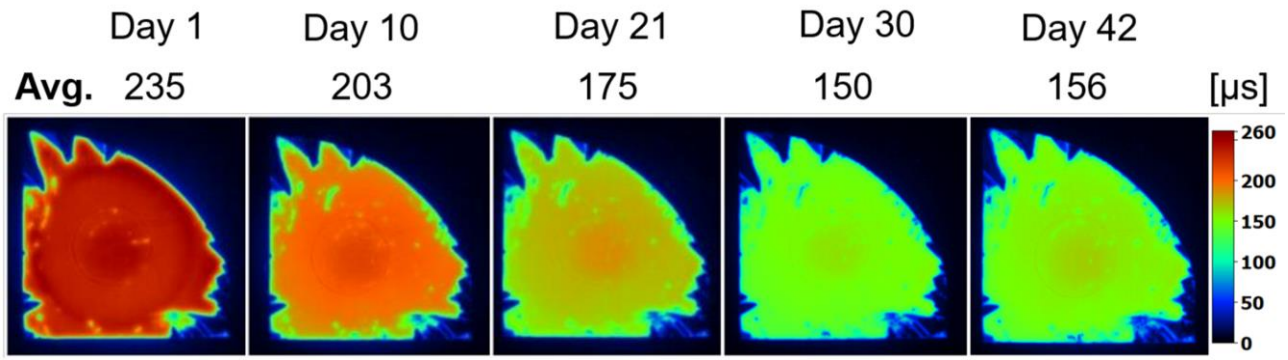

Figure 3 PL images of n-type Si wafer passivated with PEDOT:PSS over the course of 42 days. Reproduced from [41].

The stability studies of the n-type and p-type FZ-Si passivated surfaces have been performed qualitatively, as depicted in Figure 4. The longest lifetime was observed in n-Si passivated by PEDOT:PSS, whereas in p-Si, the absolute values of the lifetime were smaller. Within the first 50 days, the charge carrier lifetime decreased to about 50% in both n-type and p-type Si, which later stabilized, as observed in Figure 4, where the lines are exponential fits to the measured decay, showing consistent results with Figure 3.

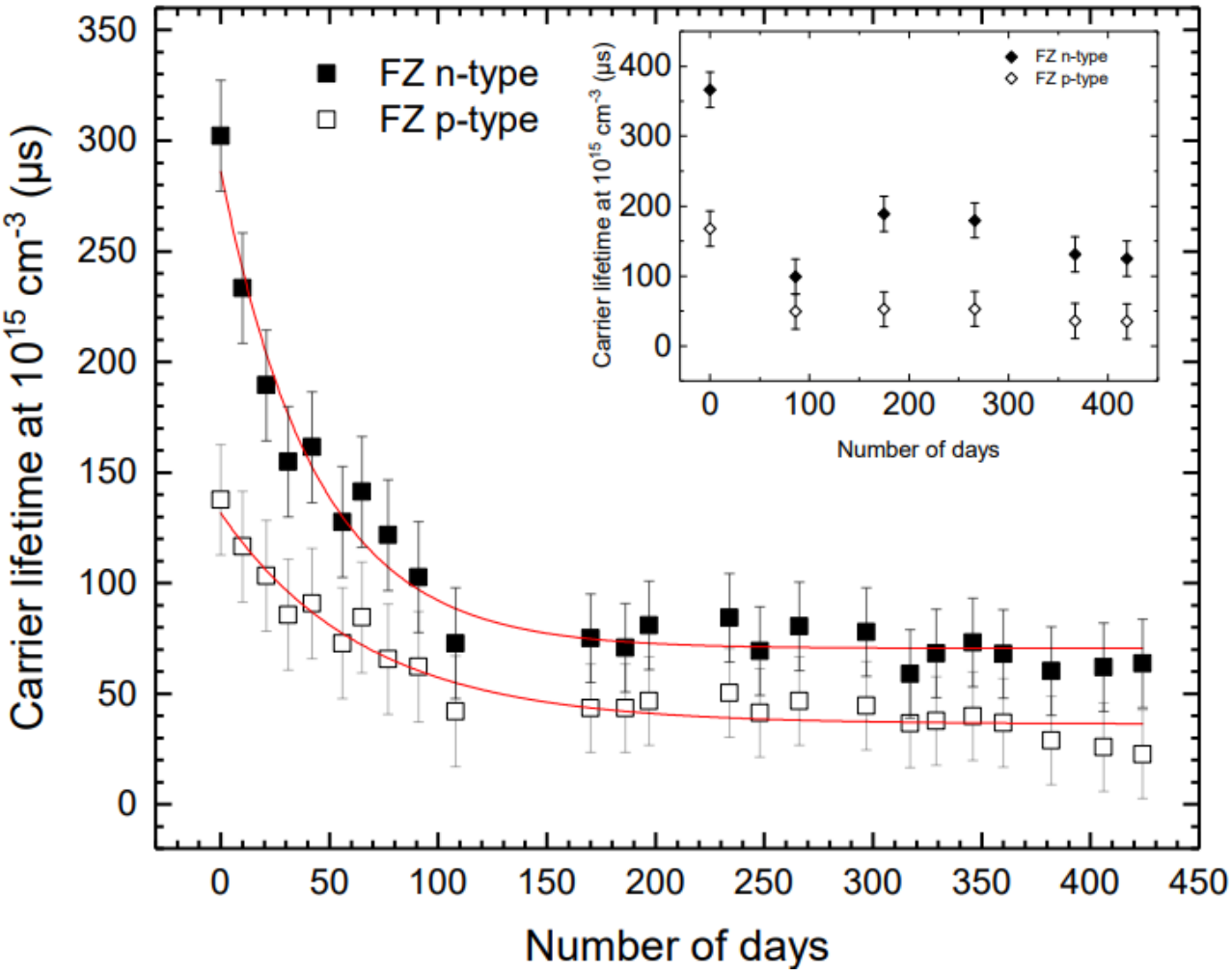

Figure 4 Measured carrier lifetime at an injection level of $1 \cdot 10^{15}$ cm^{-3} for FZ n-and p-type Si wafers passivated with PEDOT:PSS on both sides. The inset shows similar samples with longer intervals between the measurements and displaying similar degradation. Reproduced from [41].

Although all films do degrade with time, many conditions lead to long-term surface passivation with sufficient quality for high-efficiency silicon-based hybrid solar cells. Surface passivation was studied in different climatic conditions (Figure 5). In addition, the pathways to maintain improved surface passivation in a finished device were also determined.

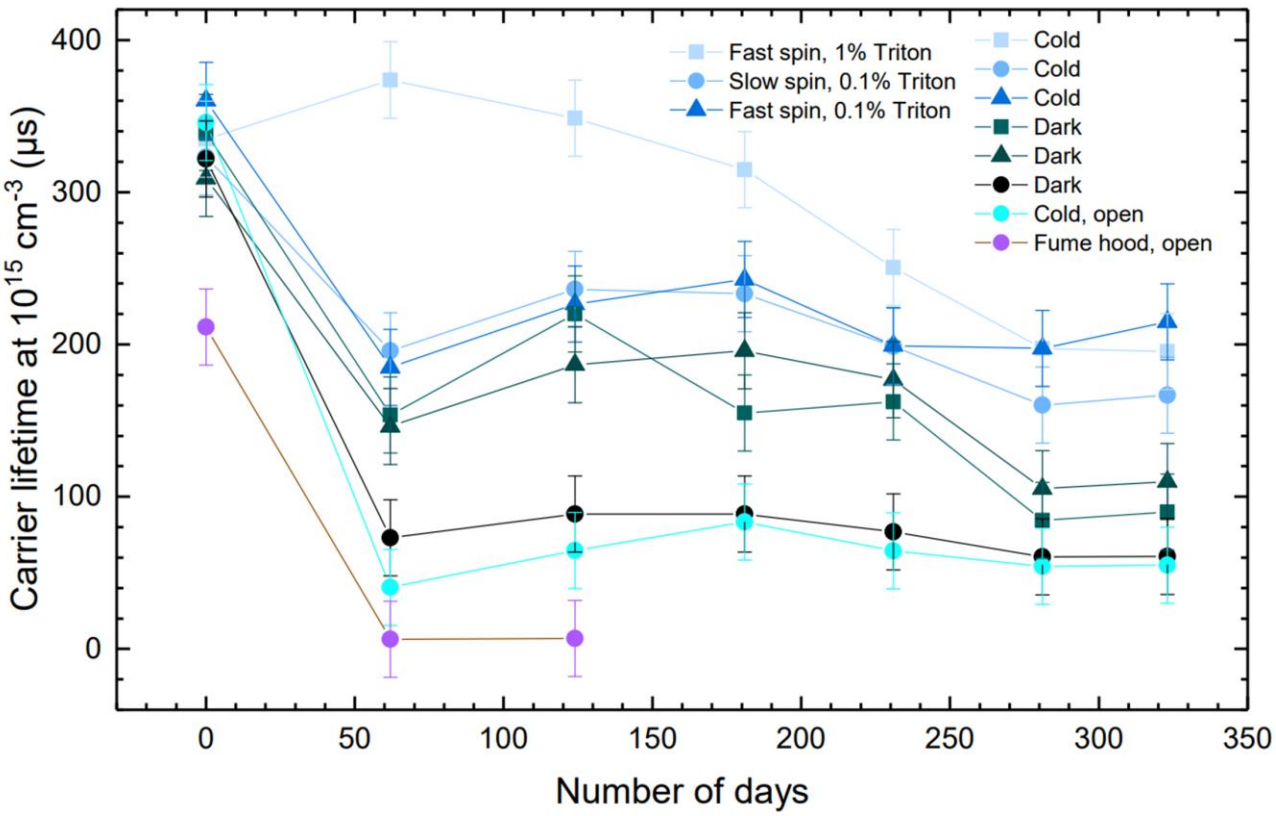

Figure 5 Measured carrier lifetime at an injection level of $1 \cdot 10^{15}$ cm^{-3} for FZ n-type Si wafers passivated with PEDOT:PSS on both sides. The wafers were fabricated slightly differently and stored at different conditions – in a fridge (cold), in a dark cupboard (dark), and exposed inside a fume hood. It appeared that storing the wafers in the cold condition provided the best stability, especially in combination with 1% Triton X-100 in the PEDOT:PSS solution. Reproduced from [41].

Current (J) voltage (V) dependence (J-V) was studied for the PEDOT:PSS/Si heterojunction. The appearance of the S-shaped J-V dependence curve was attributed to the mismatch between the energy levels of the absorber layer and the charge extraction layer, or the contact interface, resulting in a barrier for charge extraction. Energy onset at the interface of PEDOT:PSS corresponded to the hole injection barrier at the acceptor–donor interface. A reduction in this barrier decreased the series resistance and thus lowered the S-shaped behavior. Additionally, a reduction in the thickness of passivating, charge blocking, or buffer layer was shown to mitigate the S-shaped curve, as observed in Figure 6.

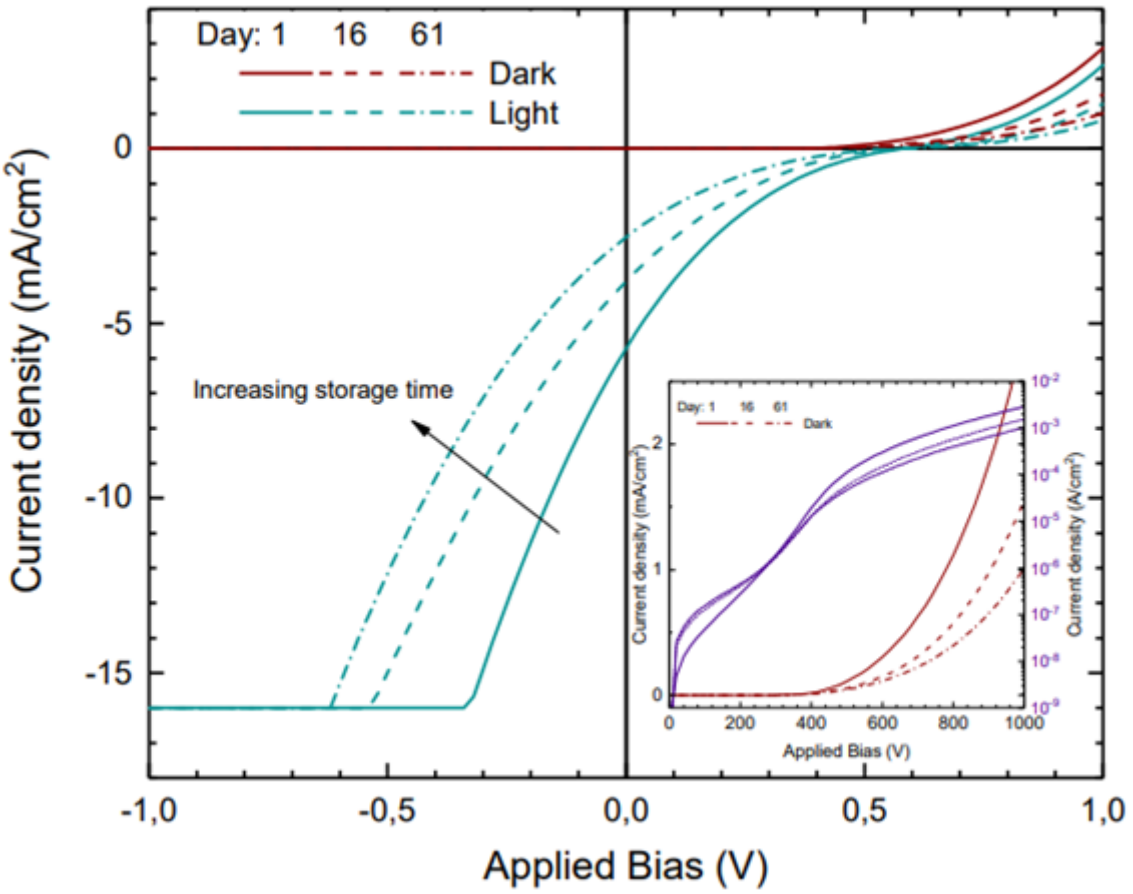

Figure 6 Current-voltage dependence in the PEDOT:PSS/Si heterojunction. Reproduced from [41].

3.1.2 PEDOT:PSS with SnO, SnO_2, and TiO_2

SnO is one of the few p-type semiconducting oxides with a bandgap in the range of 2.7–3.4 eV, which shows promising applications in solar cells and Li-ion batteries. However, its low stability due to easy oxidization to a more stable rutile phase SnO_2 limits its applicability. SnO-based composites have been studied previously [34], where 1% wt. SnO was added to the PEDOT:PSS based-mixture, as mentioned in section 2.2, and deposited over n-type Si.

The hybrid composite showed good transparency in the visible range and slight improvement in the absorption in the range of 350–450 nm in comparison to the bare PEDOT:PSS, as observed in Figure 7(a). Besides, the electrical conductivity was increased from $1.89 \cdot 10^2$ to $6.33 \cdot 10^2$ Ω^{-1} cm^{-1} (Table 1)observed from $1.89 \cdot 10^2$ to $6.33 \cdot 10^2$ Ω^{-1} cm^{-1} (Table 1) when SnO nanoparticles were added. This increase in the conductivity was accompanied by changes in the Raman spectra of the hybrid composite. The initial PEDOT:PSS-based mixture without nanoparticles was irradiated with a UV laser (λ = 325 nm) and different filters were used during the illumination to evaluate possible light-induced degradation effects, while the Raman spectra after illumination were collected with a red laser (λ = 633 nm) and a constant filter. The same process was repeated for the composite with SnO nanoparticles. According to Figure 7 (b), irrespective of the laser intensity, similar Raman signals were observed for the hybrid composites, exhibiting differences when compared to the PEDOT:PSS without nanoparticles (Figure 7(c)). This effect could be understood based on conformational changes in the polymer coils due to electrostatic interactions between surface-charged SnO

nanoparticles and the polymer matrix [18]. However, this interaction proved beneficial for the composite since it not only showed higher stability under irradiation but also a conductivity enhancement. It should be noted that the oxidation of SnO to SnO_2 was prevented during the experiments as no significant oxidation effects were observed in the Raman analysis after continuous laser irradiation of the SnO nanoparticles embedded in the polymeric matrix.

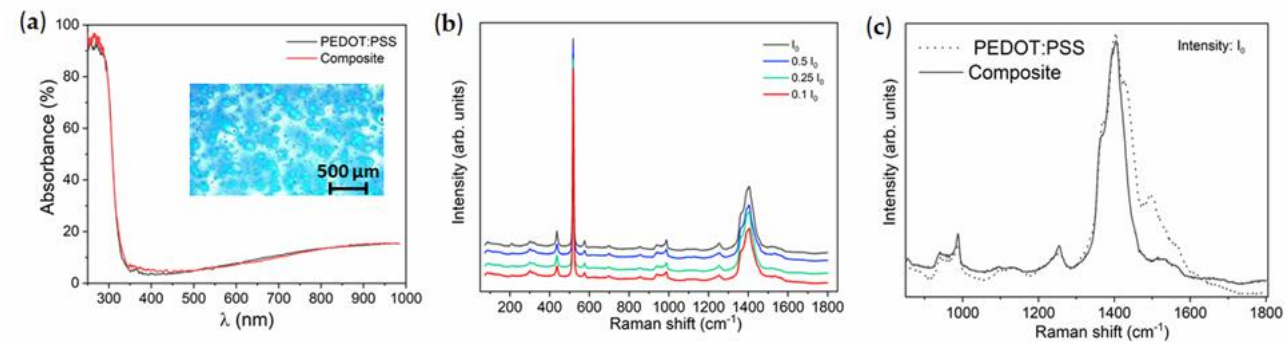

Figure 7 (a) Absorption spectra of PEDOT:PSS and hybrid composites and the optical image of the composite in the inset, **(b)** Raman spectra of the hybrid composite acquired with variable UV laser intensity, and **(c)** Raman spectra of the bare PEDOT:PSS and the hybrid composite acquired using the same laser intensity (I_0). Reproduced with permission from [34]. Synergetic Improvement of Stability and Conductivity of Hybrid Composites formed by PEDOT:PSS and SnO Nanoparticles, Vázquez-López, A., Yaseen, A., Maestre, D., Ramírez-Castellanos, J., et al.,. Molecules 2020, 25, 695 from MDPI.

Si passivation behavior of these hybrid composites was also studied by PL and QSS-PC lifetime, as shown in Figure 8. In this case, the average carrier lifetimes of 410 µs and 308 µs were estimated for PEDOT:PSS and composites with SnO, respectively. The results further confirmed that SnO composites showed a worse passivation behavior in comparison to PEDOT:PSS, which was further diminished with the use of SnO_2 in the hybrid composite, as observed in Figure 8(c). Despite the reduced lifetime, these composites were still optimal for application in solar cells due to the increased conductivity.

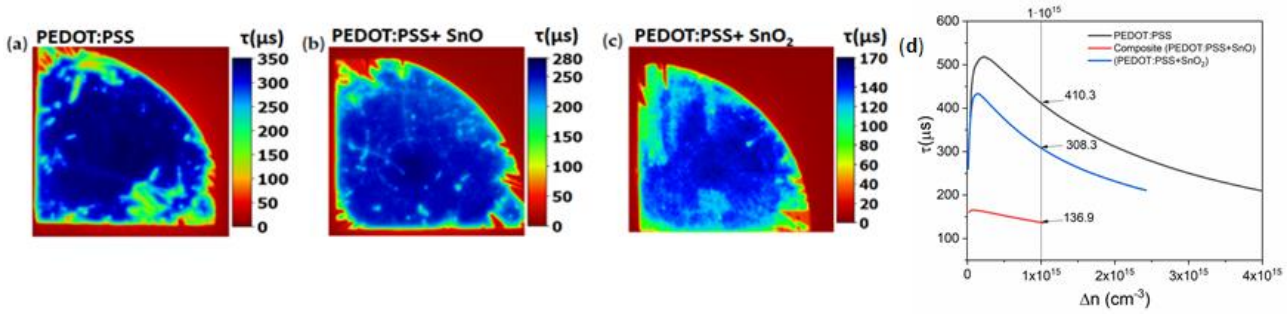

Figure 8 PL images and quasi-steady-state photoconductance (QSS-PC) lifetime values of **(a)** PEDOT:PSS, **(b)** hybrid composite, **(c)** results from an analogous hybrid composite using SnO_2 nanoparticles (1% wt.), included for comparison, and **(d)** the corresponding QSSPC graph. Reproduced from [34]., Synergetic Improvement of Stability and Conductivity of Hybrid Composites formed by PEDOT:PSS and SnO Nanoparticles,

Vázquez-López, A., Yaseen, A., Maestre, D., Ramírez-Castellanos, J., et al., Molecules 2020, 25, 695 from MDPI.

TiO_2-based composites were also studied, as reported in an earlier study [36]. TiO_2 (titania, titanium dioxide) is a well-known n-type semiconductor, with potential applications in optoelectronic devices, gas sensors, and photocatalysis. TiO_2 exists in different crystallographic structures, two metastable (anatase tetragonal, $I4_1/amd$, E_g = 3.2 eV at RT and brookite, orthorhombic, Pbca) and one stable (rutile, tetragonal, $P4_2/mnm$, E_g = 3.05 eV at RT) [42]. In the present review, anatase TiO_2 nanoparticles were chosen due to their superior optoelectronic properties. The Si passivation behavior was analyzed for anatase TiO_2-based composites via QSS-PC-calibrated PL images. Enhanced carrier lifetime values of τ= ~0.5 ms were obtained by adding a controlled amount of TiO_2 nanoparticles (0.5% wt.) to the PEDOT:PSS matrix for an injection level of $0.5 \cdot 10^{15}$ cm^{-3}. As observed in Figure 9, the lifetime values decreased with the addition of TiO_2 in concentrations over 0.5 wt %. Also, an increase in the conductivity of the hybrid composite, compared to the PEDOT:PSS, was achieved by using oxide nanoparticles (Table 1). Hence, an improved passivation behavior could be achieved by selecting the proper concentration of nanoparticles in the polymeric matrix.

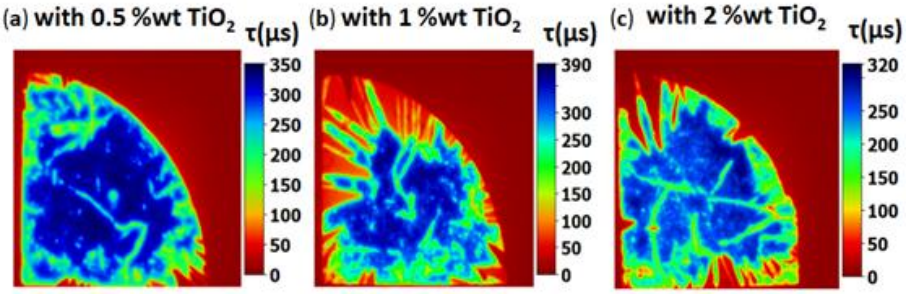

Figure 9. PL images of the composites with different concentrations of TiO_2 nanoparticles **(a)** 0.5% wt., **(b)** 1% wt., and **(c)** 2% wt. Reprinted with permission from [36]. Journal of Materials Letters, 271, Vázquez-López, A., Yaseen, A., Maestre, D., Ramírez-Castellanos, J., et al. , Improved silicon surface passivation by hybrid composites formed by PEDOT:PSS with anatase TiO_2 nanoparticles, Pages 127802., Copyright 2020, with permission from Elsevier.

Table 1 Hall effect measurements for bare PEDOT:PSS and hybrid composites measured at I = 0.1 mA, obtained [34], Synergetic Improvement of Stability and Conductivity of Hybrid Composites formed by PEDOT:PSS and SnO Nanoparticles, Vázquez-López, A., Yaseen, A., Maestre, D., Ramírez-Castellanos, J., et al., Molecules 2020, 25, 695 from MDPI. and reprinted from [36]., Journal of Materials Letters, 271, Vázquez-López, A., Yaseen, A., Maestre, D., Ramírez-Castellanos, J., et al. , Improved silicon surface passivation by hybrid composites formed by PEDOT:PSS with anatase TiO_2 nanoparticles, Pages 127802., Copyright 2020, with permission from Elsevier.

Sample	**Charge carrier concentration (cm^{-3})**	**Conductivity σ (Ω^{-1} cm^{-1})**
PEDOT:PSS	$(7.37 \pm 1.38) \cdot 10^{21}$	$(1.89 \pm 0.01) \cdot 10^{2}$

PEDOT:PSS + 0.5%wt TiO_2	$(2.99 \pm 0.71) \cdot 10^{21}$	$(2.33 \pm 0.03) \cdot 10^{2}$
PEDOT:PSS + 1%wt TiO_2	$(1.24 \pm 0.38) \cdot 10^{21}$	$(1.92 \pm 0.05) \cdot 10^{2}$
PEDOT:PSS + 2%wt TiO_2	$(1.30 \pm 0.49) \cdot 10^{22}$	$(4.39 \pm 0.03) \cdot 10^{2}$
PEDOT:PSS + 1%wt SnO	$(1.41 \pm 0.27) \cdot 10^{22}$	$(6.33 \pm 0.01) \cdot 10^{2}$

3.1.3 PEDOT:PSS with β-and γ-Ga_2O_3 Nanoparticles

β-or γ-Ga_2O_3 nanoparticles were also studied to enhance the optoelectronic properties of PEDOT:PSS. Three different methods were followed to incorporate these nanoparticles into the PEDOT:PSS as described in [37]. The first method (β-A) involved mixing of PEDOT:PSS, 5% wt. of DMSO, and 0.1% of Triton X-100 followed by stirring and filtration. Later, 1% wt. β-Ga_2O_3 nanoparticles were added to the filtered solution. In the second method (β-B or γ-B), a solution of PEDOT:PSS with 0.1% wt. of Triton X-100 and another solution containing DMSO and β- or γ-Ga_2O_3 nanoparticles in a weight ratio of 5:1 were taken separately and then mixed and stirred. In the third method (γ-C), a solution of PEDOT:PSS and 5% DMSO was filtered, followed by the addition of 0.1% wt. Triton X-100 and 1% wt. of γ-Ga_2O_3 nanoparticles. Finally, the solution was stirred and sonicated. In order to compare the results, a reference sample without nanoparticles was prepared using method C. The composites were deposited on an n-type FZ Si wafer by spin-coating.

The properties of thin layers of the composite deposited on the Si wafer were characterized by studying the charge carrier lifetime, sheet resistance, and I-V curves of the thin layers. Figure 10 shows the PL decay maps of samples β-A, β-B, γ-C, and γ-B. The results, in general, showed similar lifetime values for all samples. Moreover, the darker colors in Figure 10(c) indicate that the γ-C sample had the longest lifetime of 335 µs. The quantitative lifetime values of the four samples are listed in Table 2. In addition to the lifetime values, the sheet resistance values were also measured for these samples, where the γ-C sample showed the highest value, while the β-A exhibited the lowest one (Table 2).

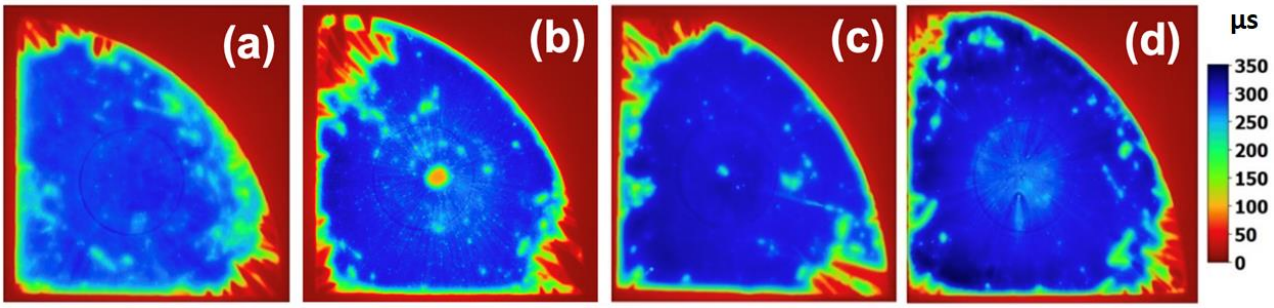

Figure 10 PL images of samples **(a)** β-A, **(b)** β-B, **(c)** γ-C, and **(d)** γ-B. Reprinted from [37]. Journal of Materials Letters, 261, García-Carrión, M., Ramírez-Castellanos, J., Nogales, E., Méndez, B., et al., Hybrid solar cells with β-and γ-gallium oxide nanoparticles, Pages 127088., Copyright 2020, with permission from Elsevier.

Table 2 Properties of PEDOT:PSS/Ga_2O_3 nanoparticle composite. Reprinted from [37], Journal of Materials Letters, 261, García-Carrión, M., Ramírez-Castellanos, J., Nogales,

E., Méndez, B., et al., Hybrid solar cells with β-and γ-gallium oxide nanoparticles, Pages 127088., Copyright 2020, with permission from Elsevier..

Sample	τ (μs)	R_{sheet} (KΩ/sq)
β-A	288	1.15 ±0.10
β-B	301	1.13 ±0.10
γ-C	335	5.15 ±0.10
γ-B	309	3.17 ±0.10
PEDOT:PSS (reference)	310	0.75 ±0.10

Finally, the I-V characteristics of the composite layers were investigated. In order to achieve this, Ag contacts were made on the composite thin layer, as shown in Figure 11(c). The I-V curves under dark conditions for samples β-A, β-B, and γ-C, γ-B are shown in Figure 11(a) and (b), respectively. The behavior was characteristic of a Schottky contact, as expected [22]. In all the cases, better results were obtained for the hybrid layers of samples β-A and γ-B than the reference PEDOT:PSS sample prepared without nanoparticles by following the same procedure.

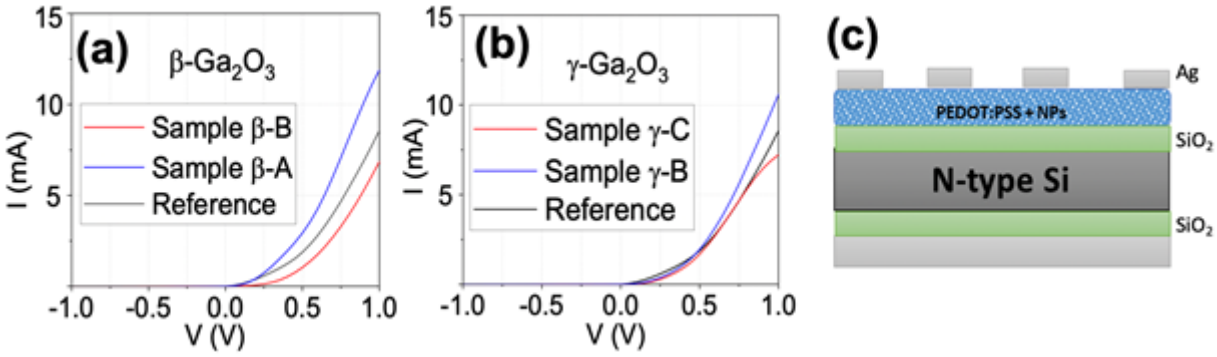

Figure 11 a) and **(b)** I-V curves of PEDOT:PSS with Ga_2O_3 NPs and the reference sample, and **(c)** the contact montage scheme, Reprinted from [37]., Journal of Materials Letters, 261, García-Carrión, M., Ramírez-Castellanos, J., Nogales, E., Méndez, B., et al., Hybrid solar cells with β-and γ-gallium oxide nanoparticles, Pages 127088., Copyright 2020, with permission from Elsevier.

3.1.4 Electrical and Optical Properties of Thin Films of the PEDOT:PSS/NiO Composite

A p-type semiconductor oxide, such as NiO, was incorporated into PEDOT:PSS. Next, PEDOT:PSS was mixed with DMSO and, as reported, superior conductivity was obtained. However, other organic solvents could also be used. In the present case, PEDOT:PSS was mixed with Triton X-100 and DMSO or EG to obtain a homogenous film that could passivate the Si surface with a charge carrier lifetime of 300–400 μs along with good reproducibility [43]. The surfactants like DMSO or EG did not change the optical properties of PEDOT:PSS (Figure 12(a)). However, Si surface passivation was changed substantially (Figure 12(b)) at low injection levels.

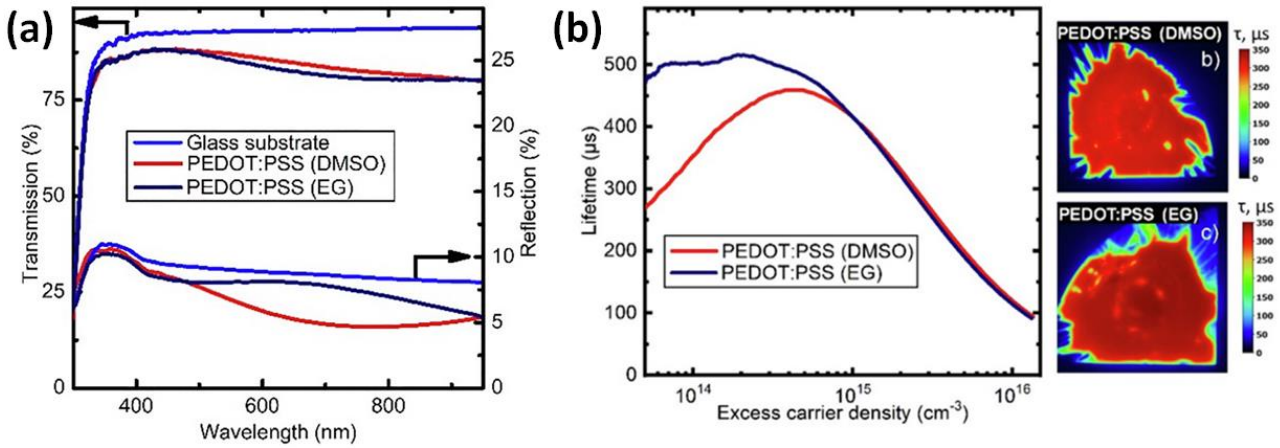

Figure 12(a) Optical properties of PEDOT: PSS (DMSO) and PEDOT: PSS (EG) and **(b)** charge carrier lifetime in PEDOT:PSS (DMSO) and PEDOT: PSS (EG). Reprinted from [44]. Mater. Today Proc, Author(s), Moldarev, D., Taeño, M., Maestre, D., Cremades, A., et al., Electrical and optical properties of composite PEDOT:PSS-based thin films with NiO nanoparticles, Copyright 2020, with permission from Elsevier.

Si surface passivation properties, most of the time, strongly depended on the surfactants (Figure 13(a)) and NiO nanoparticle concentration (Figure 13(b)) [43]. Furthermore, there was a high possibility of degradation of the passivation properties in the air, whereas, in the N_2 atmosphere, charge carrier lifetime saturated at 150 µs. Also, the lifetime values worsened further (Figure 13(b)), probably due to the formation of large-sized agglomerates exceeding the film thickness.

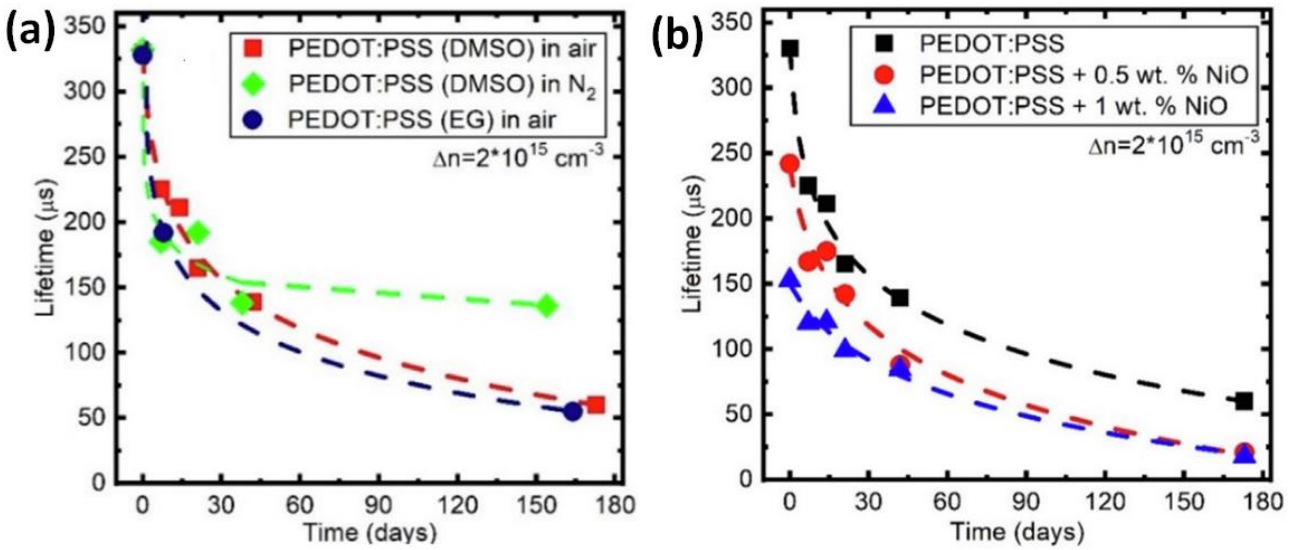

Figure 13 Time-resolved measurements of the lifetime for PEDOT:PSS with **(a)** DMSO in the air and N_2 and EG in the air and **(b)** pure PEDOT:PSS and NiO-doped PEDOT:PSS. Reprinted from [43]. , Mater. Today Proc, Author(s), Moldarev, D., Taeño, M., Maestre, D., Cremades, A., et al., Electrical and optical properties of composite PEDOT:PSS-based thin films with NiO nanoparticles, Copyright 2020, with permission from Elsevier.

3.1.5 Incorporation of Si-nanoparticles in PEDOT:PSS for Si Surface Passivation

Si-nanoparticles containing the PEDOT:PSS composite were spin-coated on the top of the n-Si wafer [44]. Although the composite enhanced the Si surface passivation by increasing the carrier lifetime from 320 µs to 420 µs at a minority carrier injection level of $2 \cdot 10^{15}$ cm^{-3}, it did not change the kinetics of the carrier lifetime degradation considerably. Figure 14 shows the time dependence of charge carrier lifetime as a function of temperature for composites with variable concentrations of Si nanoparticles.

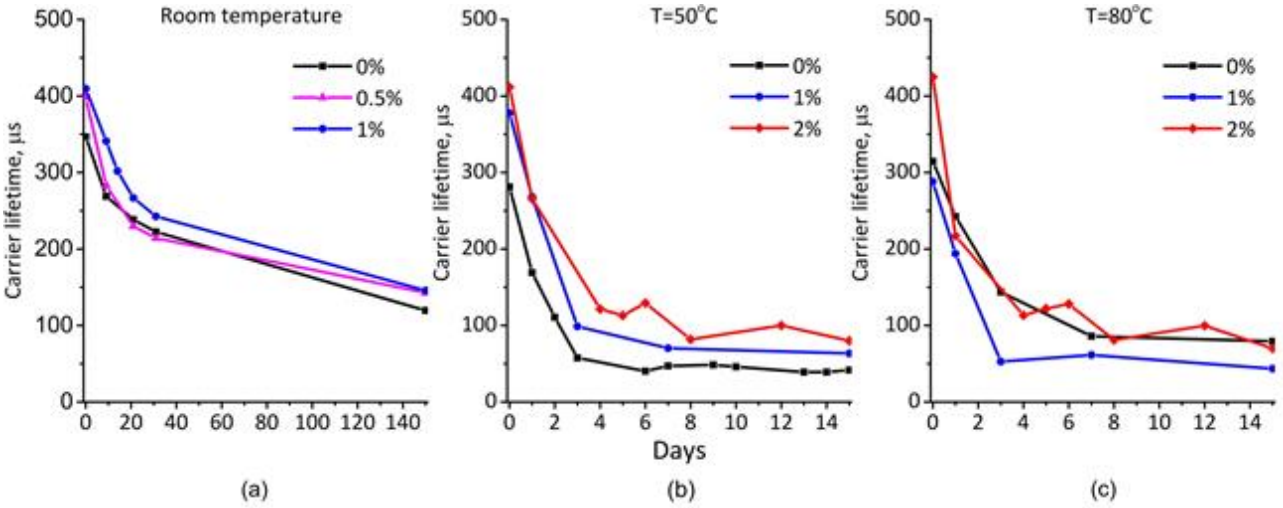

Figure 14 Time dependence of charge carrier lifetime for the hybrid/composite of PEDOT:PSS and Si nanoparticles with temperatures reprinted from [44]. , Mater. Today Proc, Mater. Today Proc, Influence of Si-nanoparticles on PEDOT:PSS properties for hybrid solar cells, Copyright 2020, with permission from Elsevier.

3.2 Hybrid Composites for Li-ion Batteries

Li-ion batteries have been established as the main energy storage devices during the past decades. The most commonly used anodes are based on carbon allotropies, which exhibit a low specific capacity (around 372 mAh/g). This raised the need to discover novel materials that can be used as negative electrodes to achieve high performance. Silicon and transition metal oxides possess higher specific capacities than carbon-based materials. Del Prado [25] et al. showed that SnO_2 and TiO_2 as anodes in Li-ion batteries could show specific capacities of ~615 mAh/g and ~125 mAh/g, respectively. Si, with an extremely high theoretical capacity (3576 mAh/g at RT), exhibits attractive cycling capacity. Although it has a specific capacity almost 10 times higher than the commercial graphite-based anodes, it still presents some challenges, including low conductivity that must be overcome for its commercialization.

Conventional electrodes generally consist of active material, a conductive additive, and a polymeric binder. When the conductive additive and binder are used, they significantly reduce the volumetric and gravimetric capacity of the electrode. Therefore, it was reported that only the conductive polymer should be used instead of both conductive additive and conventional binder [45]. Previous studies have investigated the performance of the Si anode with different kinds of binders, including conductive polymers and their combinations [46-50].

In the present review, the conductivity of the Si electrode in combination with different polymers and their effects on the Li-ion battery performance were summarized (Figure 15). In Figure 15(a) and (b), the cycling performance of Si with PEDOT:PSS and PEDOT:PSS (Heraus), respectively, showed that the different behaviors of electrodes were ascribed to the conductivities of the two types of PEDOT:PSS polymers used. Si was used with the PAA/PVA binder and conductivity of the electrode was provided by carbon black (CB) and carbon nanotube (CNT) (Figure 15(c)). The specific capacities after 100 cycles at C/5 were found to be 1071, 1560, and 1506 mAh/g for Si/PEDOT:PSS, Si/PEDOT:PSS (Heraus), and Si/PAA-PVA/CB/CNT, respectively. These results showed that the electrodes with conductive PEDOT:PSS and non-conductive binder combination showed very similar values of specific capacities, whereas an electrode with only conductive polymer (Si/PEDOT:PSS (Heraus)) showed a high volumetric capacity of 566 mAh/cm^3 after 100 cycles, in comparison to 363 mAh/cm^3 for Si/PEDOT:PSS and 558 mAh/cm^3 for Si/PAA-PVA/CB/CNT. The other advantage of using the conductive polymer only with Si was the easy electrode preparation process to get a homogeneous electrode slurry due to the hydrophobic properties of CB and CNT.

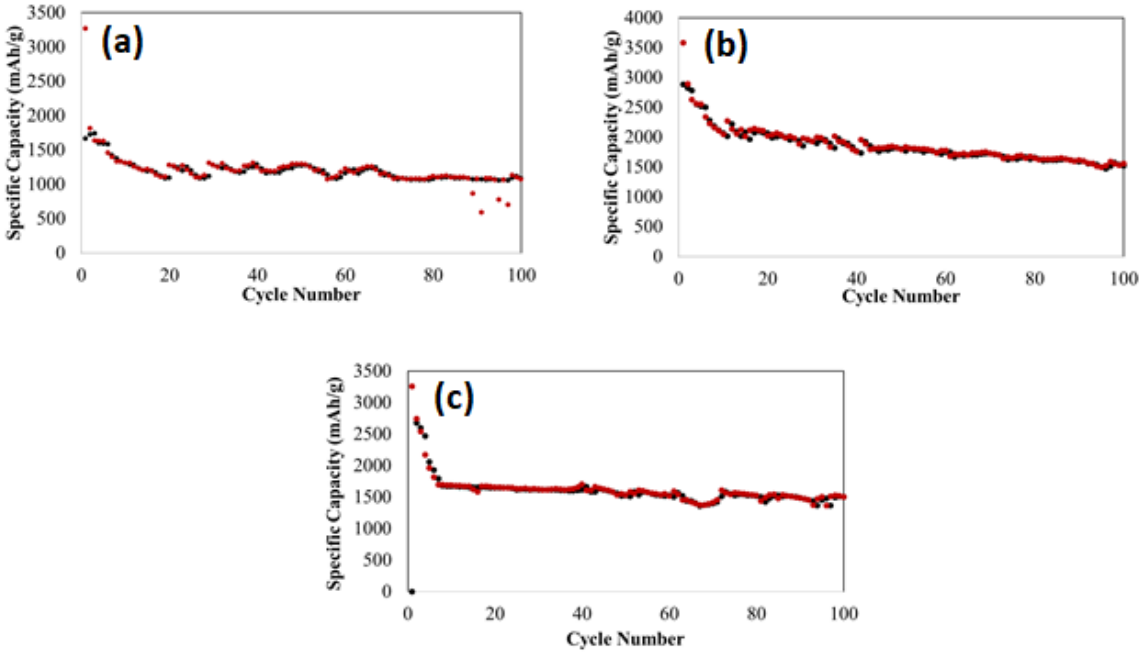

Figure 15 Cycling performance of **(a)** Si/PEDOT:PSS, **(b)** Si/PEDOT:PSS (Heraus), and **(c)** Si/PAA-PVA/CB/CNT.

Although Si-based anodes in Li-ion batteries have been studied enormously, improvement in the cycling stability of the batteries still needs to be investigated further. For this purpose, transition metal oxides have been regarded as important anode candidates for achieving high-performance Li-ion batteries. TiO_2, one of the main candidates, has been investigated widely, owing to its cycle stability, chemical inertness, and high safety [51-54]. It is well known that the optoelectronic properties of nanoparticles depend on the morphology and size or volume-surface ratio, and thus, can be modified by doping these nanomaterials with other elements [23, 35].

Herein, we summarized a few studies on the doping of TiO_2 with Li metal. In one of the studies, TiO_2 was doped with 20% wt. and 30% wt. Li (labeled as 0.2Li and 0.3 Li), and then used as the anode material. In order to prepare the Li-doped TiO_2, a diluted stoichiometric quantity of Li was added

using a method similar to the one explained in [35]. The cycling results of TiO_2, TiO_2(0.2Li), and TiO_2(0.3Li), shown in Figure 16**,** revealed that after 200 cycles at C/5, cells with TiO2, TiO_2(0.2Li), and TiO_2(0.3Li) electrodes exhibited the cyclic capacities of 225, 261, and 396 mAh/g, respectively. The results from other studies show that TiO_2 doped with other materials including graphene and Si could be a potential anodic material for Li-ion batteries due to its excellent stability [54-56].

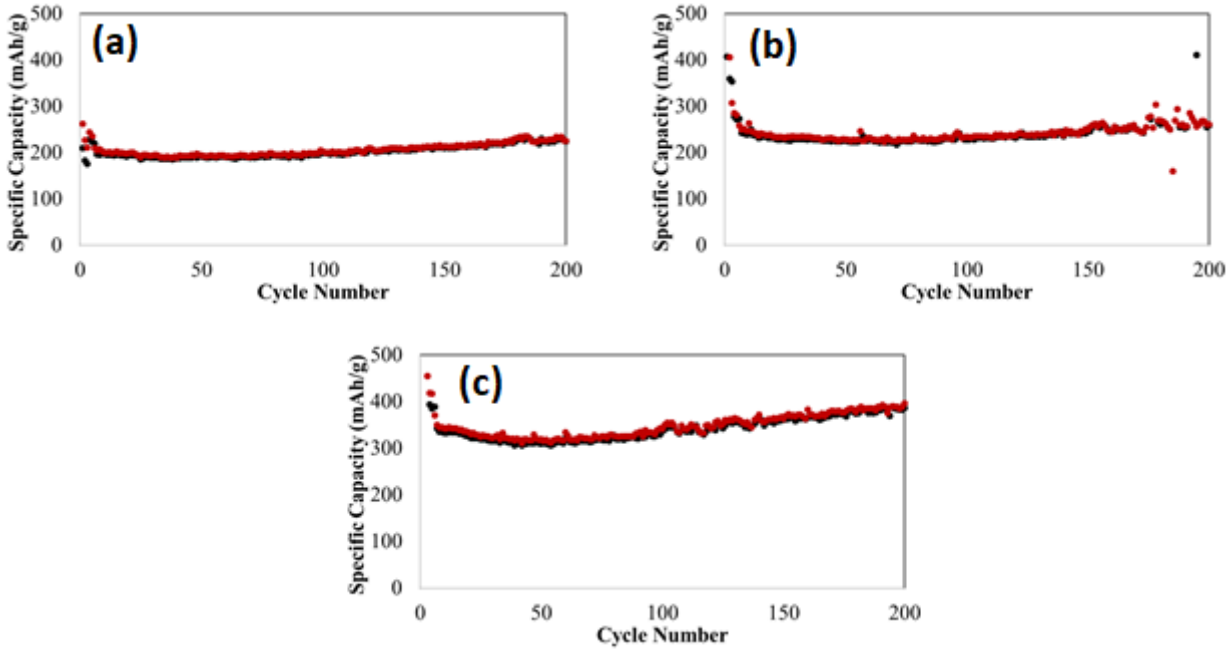

Figure 16 Cycling performance of **(a)** TiO_2, **(b)** TiO_2 (0.2Li), and **(c)** TiO_2(0.3Li).

Similarly, SnO_2 has also been evaluated as a possible anode material for Li-ion batteries[35]. Briefly, the cycling performance of the batteries comprising SnO_2-based active materials, binder, and carbon black (CB) mixed in water, with the optimized weight ratio of SnO_2 nanoparticle/PAA/CB = 70/20/10, and SnO_2 doped with Li or Ni (20% wt. or 30% wt.) were investigated (Figure 17). The specific capacity measurement results showed that undoped SnO_2 nanoparticles and the one doped with 30% wt. Li exhibited the highest capacity values of about 600 mAh/g after 100 cycles. The resulting capacity and the electrical, morphological, and luminescent properties showed that the charge state of the dopants influenced the cycling performance and must be taken into account during the synthesis of these anodes.

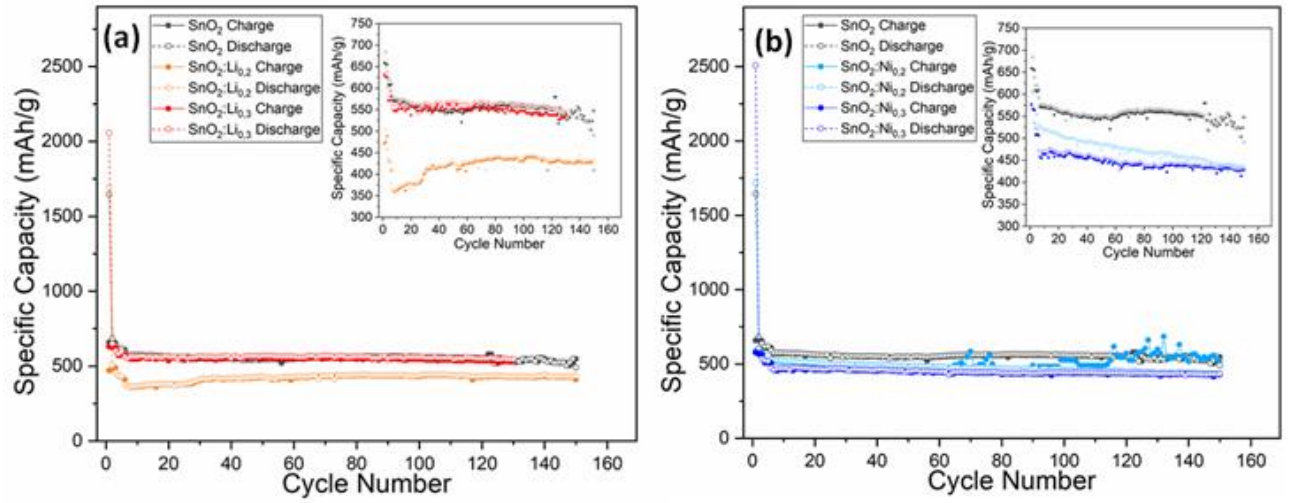

Figure 17 Cycling performance of **(a)** SnO_2, SnO_2 (0.2Li), SnO_2(0.3Li) and **(b)** SnO_2, SnO_2 (0.2Ni) and SnO_2(0.3Ni). Reprinted with permission from Vázquez-López, A., Maestre, D., Ramírez-Castellanos, J., González-Calbet, J.M., et al., Influence of Doping and Controlled Sn Charge State on the Properties and Performance of SnO_2 Nanoparticles as Anodes in Li-Ion Batteries. J. Phys. Chem. C 2020, 124, 18490–18501 Copyright (2020) American Chemical Society [35].

4. Conclusions

Hybrid materials are gaining continuous attention in the scientific community due to their synergetic and tailored properties as well as low-cost processing and scalability. In this review, we summarized our recent research on the synthesis and characterization of hybrid composites and nanomaterials for silicon passivation in photovoltaic devices and utilization as anode materials in Li-ion batteries. The organic component of the investigated hybrid composites consisted of the conductive polymer PEDOT:PSS with some selected additives. Diverse nanomaterials (Si, SnO_2, SnO, TiO_2, NiO, and Ga_2O_3) were synthesized and embedded in the polymeric matrix as inorganic counterparts. SnO-based composites showed an improved conductivity in comparison to the unfunctionalized PEDOT:PSS due to a synergetic effect, preventing the oxidation of SnO to SnO_2. The addition of Ga_2O_3 and anatase TiO_2 to the PEDOT:PSS improved carrier lifetime values compared to bare PEDOT:PSS. Also, the addition of Si nanoparticles to the hybrid composite increased the charge carrier recombination lifetime up to 420 µs. Furthermore, the stability of thin layers of these hybrid materials on the surface of different substrates, including n-and p-type FZ Si was evaluated. The use of semiconductor oxide nanoparticles in the composite not only enhanced their electrical conductivity but also increased the lifetime of the charge carriers, leading to improved cyclic performance with potential applicability in hybrid solar cell devices.

Besides, TiO_2, SnO_2, and Si were evaluated as possible active anode materials in Li-ion batteries. Si exhibited improved specific capacity and stability with bare PEDOT:PSS as the conductive polymer without any binders or conductive additives. Anodes based on undoped or Li-doped TiO_2 and SnO_2 showed improved capacities of around 400 and 600 mAh/g, respectively. All anode materials were stable up to 150 cycles and were considered safe materials.

Hence, with their unique synergistic properties achieved by the controlled addition of nanomaterials to the polymeric matrix, hybrid composites have demonstrated potential for

applications in energy storage devices, such as solar cells and Li-ion batteries. These promising results could extend the use of these versatile hybrid materials in other research areas.

Acknowledgments

This work was supported by projects RTI2018-097195-B-I00, and M-ERA.NET PCIN-2017-106, from the Spanish Ministry of Innovation, Science, and Technology and the Spanish Ministry of Economy, M-ERA.net project 272806 by the Research Council of Norway, and M-ERA.net project by TUBITAK.

Author Contributions

Antonio Vázquez-López, Marina García-Carrión, María Taeño carried the nanoparticles synthesis under the supervision of Julio Ramírez-Castellanos, and carried the characterization under the supervision of David Maestre, Emilio Nogales, Pedro Hidalgo, Bianchi Méndez, and Ana Cremades

Antonio Vázquez-López, Marina García-Carrión, Erlend Hall, Anisa Yaseen assembled and characterised composites based on PEDOT:PSS under the supervision of Smagul Karazhanov, Erik S. Marstein. Junjie Zhu, Xinyu Zhang kindly provided half solar cells for deposition.

Ilknur Kalafat, Elif Arici, Omer Suat Taskin contributed to the assembly, design, data acquisition and analysis of the cells mentioned in this work under the supervision of Neslihan Yuca.

Funding acquisition and project administration was directed under B. Méndez, N. Yuca, S. Zh. Karazhanov, E.S. Marstein, A. Cremades

Funding

The Spanish Ministry of Innovation, Science, and Technology and the Spanish Ministry of Economy through Research Projects RTI2018-097195-B-I00, and M-ERA.NET PCIN-2017-106 funded this research. IFE has received financial support from the M-ERA.net project 272806 by the Research Council of Norway. ENWAIR has received financial support from M-ERA.net project by TUBITAK.

Competing Interests

The authors have declared that no competing interests exist.

References

1. Park SY, Lee JE, Kim YH, Kim JJ, Shim YS, Kim SY, et al. Room temperature humidity sensors based on rGO/MoS_2 hybrid composites synthesized by hydrothermal method. Sens Actuators B Chem. 2018; 258: 775-782.
2. Wang S, Kang Y, Wang L, Zhang H, Wang Y, Wang Y. Organic/inorganic hybrid sensors: A review. Sens Actuators B Chem. 2013; 182: 467-481.
3. Fan Q, Zhang Q, Zhou W, Xia X, Yang F, Zhang N, et al. Novel approach to enhance efficiency of hybrid silicon-based solar cells via synergistic effects of polymer and carbon nanotube composite film. Nano Energy. 2017; 33: 436-444.
4. Magu TO, Agobi AU, HITLER L, Dass PM. A review on conducting polymers-based composites for energy storage application. J Chem Rev. 2019; 1: 19-34.

5. Sun K, Zhang S, Li P, Xia Y, Zhang X, Du D, et al. Review on application of PEDOTs and PEDOT:PSS in energy conversion and storage devices. J Mater Sci Mater Electron. 2015; 26: 4438-4462.
6. Fan Z, Ouyang J. Thermoelectric properties of PEDOT:PSS. Adv Electron Mater. 2019; 5: 1800769.
7. Hu L, Song J, Yin X, Su Z, Li Z. Research progress on polymer solar cells based on PEDOT:PSS electrodes. Polymers. 2020; 12: 145.
8. Lee CP, Lai KY, Lin CA, Li CT, Ho KC, Wu CI, et al. A paper-based electrode using a graphene dot/PEDOT:PSS composite for flexible solar cells. Nano Energy. 2017; 36: 260-267.
9. Xia Y, Dai S. Review on applications of PEDOTs and PEDOT:PSS in perovskite solar cells. J Mater Sci Mater Electron. 2020; 26: 1-12.
10. Zhang C, Zhang Y, Guo H, Jiang Q, Dong P, Zhang C. Efficient planar hybrid n-Si/PEDOT:PSS solar cells with power conversion efficiency up to 13.31% achieved by controlling the SiOx Interlayer. Energies. 2018; 11: 1397.
11. Gueye MN, Carella A, Faure-Vincent J, Demadrille R, Simonato JP. Progress in understanding structure and transport properties of PEDOT-based materials: A critical review. Prog Mater Sci. 2020; 108: 100616.
12. Khang DY. Recent progress in Si-PEDOT:PSS inorganic-organic hybrid solar cells. J Phys D Appl Phys. 2019; 52: 503002.
13. Jäckle S, Liebhaber M, Gersmann C, Mews M, Jäger K, Christiansen S, et al. Potential of PEDOT:PSS as a hole selective front contact for silicon heterojunction solar cells. Sci Rep. 2017; 7: 2170.
14. Zielke D, Pazidis A, Werner F, Schmidt J. Organic-silicon heterojunction solar cells on n-type silicon wafers: The BackPEDOT concept. Sol Energy Mater Sol Cells. 2014; 131: 110-116.
15. Lingstedt LV, Ghittorelli M, Lu H, Koutsouras DA, Marszalek T, Torricelli F, et al. Effect of DMSO solvent treatments on the performance of PEDOT:PSS based organic electrochemical transistors. Adv Electron Mater. 2019; 5: 1800804.
16. Mahato S, Puigdollers J, Voz C, Mukhopadhyay M, Mukherjee M, Hazra S. Near 5% DMSO is the best: A structural investigation of PEDOT:PSS thin films with strong emphasis on surface and interface for hybrid solar cell. Appl Surf Sci. 2020; 499: 143967.
17. Xiong S, Zhang L, Lu X. Conductivities enhancement of poly (3, 4-ethylenedioxythiophene)/poly (styrene sulfonate) transparent electrodes with diol additives. Polym Bull. 2013; 70: 237-247.
18. Shi H, Liu C, Jiang Q, Xu J. Effective approaches to improve the electrical conductivity of PEDOT:PSS: A review. Adv Electron Mater. 2015; 1: 1500017.
19. Tevi T, Saint Birch SW, Thomas SW, Takshi A. Effect of Triton X-100 on the double layer capacitance and conductivity of poly (3, 4-ethylenedioxythiophene): Poly (styrenesulfonate) (PEDOT:PSS) films. Synth Met. 2014; 191: 59-65.
20. Nagata R, Yanagi Y, Fujii S, Kataura H, Nishioka Y. Application of highly conductive DMSO-treated PEDOT:PSS electrodes to flexible organic solar cells. Proceeding of 21st International Workshop on Active-Matrix Flatpanel Displays and Devices (AM-FPD); 2014 July 2-4; Kyoto, Japan. New York: IEEE.
21. Sun Z, He Y, Xiong B, Chen S, Li M, Zhou Y, et al. Performance-enhancing approaches for PEDOT:PSS-Si hybrid solar cells. Angew Chem Int Ed. 2021; 60: 5036-5055.
22. García-Tecedor M, Karazhanov SZ, Vasquez GC, Haug H, Maestre D, Cremades A, et al. Silicon surface passivation by PEDOT:PSS functionalized by SnO_2 and TiO_2 nanoparticles. Nanotechnology. 2017; 29: 035401.

23. Savkina R, Khomenkova L. Oxide-based materials and structures. Boca Raton, FL: CRC Press; 2020.
24. Higgins TM, Park SH, King PJ, Zhang C, McEvoy N, Berner NC, et al. A commercial conducting polymer as both binder and conductive additive for silicon nanoparticle-based lithium-ion battery negative electrodes. ACS Nano. 2016; 10: 3702-3713.
25. Del Prado F, Andersen HF, Taeño M, Mæhlen JP, Ramírez-Castellanos J, Maestre D, et al. Comparative study of the implementation of tin and titanium oxide nanoparticles as electrodes materials in Li-ion batteries. Sci Rep. 2020; 10: 5503.
26. Wang X, Sun L, Sun X, Li X, He D. Size-controllable porous NiO electrodes for high-performance lithium ion battery anodes. Mater Res Bull. 2017; 96: 533-537.
27. Zoller F, Böhm D, Bein T, Fattakhova-Rohlfing D. Tin oxide based nanomaterials and their application as anodes in lithium‐ion batteries and beyond. ChemSusChem. 2019; 12: 4140-4159.
28. Zheng P, Liu T, Su Y, Zhang L, Guo S. TiO_2 nanotubes wrapped with reduced graphene oxide as a high-performance anode material for lithium-ion batteries. Sci Rep. 2016; 6: 36580.
29. Liu Y, Palmieri A, He J, Meng Y, Beauregard N, Suib SL, et al. Highly conductive In-SnO_2/RGO nano-heterostructures with improved lithium-ion battery performance. Sci Rep. 2016; 6: 25860.
30. Bonomo M. Synthesis and characterization of NiO nanostructures: A review. J Nanopart Res. 2018; 20: 222.
31. Zhao Q, Ma L, Zhang Q, Wang C, Xu X. SnO_2-based nanomaterials: Synthesis and application in lithium-ion batteries and supercapacitors. J Nanomater. 2015; 2015: 850147.
32. Chen X, Mao SS. Titanium dioxide nanomaterials: Synthesis, properties, modifications, and applications. Chem Rev. 2007; 107: 2891-2959.
33. Li L, Wei W, Behrens M. Synthesis and characterization of α-, β-, and γ-Ga_2O_3 prepared from aqueous solutions by controlled precipitation. Solid State Sci. 2012; 14: 971-981.
34. Vázquez-López A, Yaseen A, Maestre D, Ramírez-Castellanos J, Marstein ES, Karazhanov SZ, et al. Synergetic improvement of stability and conductivity of hybrid composites formed by PEDOT:PSS and SnO nanoparticles. Molecules. 2020; 25: 695.
35. Vazquez-Lopez A, Maestre D, Ramirez-Castellanos J, Gonzalez-Calbet JM, Pis I, Nappini S, et al. Influence of doping and controlled sn charge state on the properties and performance of SnO_2 nanoparticles as anodes in Li-ion batteries. J Phys Chem C. 2020; 124: 18490-18501.
36. Vázquez-López A, Yaseen A, Maestre D, Ramírez-Castellanos J, Karazhanov SZ, Marstein ES, et al. Improved silicon surface passivation by hybrid composites formed by PEDOT:PSS with anatase TiO_2 nanoparticles. Mater Lett. 2020; 271: 127802.
37. García-Carrión M, Ramírez-Castellanos J, Nogales E, Méndez B, You CC, Karazhanov S, et al. Hybrid solar cells with β-and γ-gallium oxide nanoparticles. Mater Lett. 2020; 261: 127088.
38. Taeño M, Ramírez-Castellanos J, Maestre D, Cremades A. Synthesis and characterization of NiO- and Sn-doped NiO micro and nanostructures. In: Oxide-based Materials and Devices XI. Bellingham, WA: SPIE; 2020. pp.112810Z.
39. Halbich MU, Zielke D, Gogolin R, Sauer-Stieglitz R, Lövenich W, Schmidt J. Improved surface passivation and reduced parasitic absorption in PEDOT:PSS/c-Si heterojunction solar cells through the admixture of sorbitol. Sci Rep. 2019; 9: 9755.
40. Bhowal AC, Talukdar H, Kundu S. Preparation, characterization and electrical behaviors of PEDOT:PSS-Au/Ag nanocomposite thin films: An ecofriendly approach. Polym Bull. 2019; 76: 5233-5251.

41. Hall E. Synthesis and characterisation of PEDOT:PSS/silicon interfaces for use in low cost, high efficiency solar cells. Oslo: University of Oslo; 2020.
42. Zhang Y, Jiang Z, Huang J, Lim LY, Li W, Deng J, et al. Titanate and titania nanostructured materials for environmental and energy applications: A review. RSC Adv. 2015; 5: 79479-79510.
43. Moldarev D, Taeño M, Maestre D, Cremades A, Karazhanov SZ, Marstein E. Electrical and optical properties of composite PEDOT:PSS-based thin films with NiO nanoparticles. Mater Today Proc. 2020; 33: 2499-2502.
44. Mamedov D, You CC, Karazhanov SZ, Marstein ES. Influence of Si-nanoparticles on PEDOT:PSS properties for hybrid solar cells. Mater Today Proc. 2020; 33: 2517-2519.
45. Liu G, Xun S, Vukmirovic N, Song X, Olalde-Velasco P, Zheng H, Bet al. Polymers with tailored electronic structure for high capacity lithium battery electrodes. Adv Mat Res. 2011; 23: 4679-4683.
46. Higgins TM, Park SH, King PJ, Zhang C, McEvoy N, Berner NC, et al. A commercial conducting polymer as both binder and conductive additive for silicon nanoparticle-based lithium-ion battery negative electrodes. ACS Nano. 2016; 10: 3702-3713.
47. Sengodu P, Deshmukh AD. Conducting polymers and their inorganic composites for advanced Li-ion batteries: A review. RSC Adv. 2015; 5: 42109-42130.
48. Yuca N, Cetintasoglu ME, Dogdu MF, Akbulut H, Tabanli S, Colak U, et al. Highly efficient poly (fluorene phenylene) copolymer as a new class of binder for high-capacity silicon anode in lithium-ion batteries. Int J Energy Res. 2018; 42: 1148-1157.
49. Yuca N, Çolak Ü. A facile and functional process to enhance electrochemical performance of silicon anode in lithium ion batteries. Electrochim Acta. 2016; 222: 1538-1544.
50. Wu M, Xiao X, Vukmirovic N, Xun S, Das PK, Song X, et al. Toward an ideal polymer binder design for high-capacity battery anodes. J Am Chem Soc. 2013; 135: 12048-12056.
51. Gao X, Sun X, Jiang Z, Wang Q, Gao N, Li H, et al. Introducing nanodiamond into TiO_2-based anode for improving the performance of lithium-ion batteries. New J Chem. 2019; 43: 3907-3912.
52. Madian M, Eychmüller A, Giebeler L. Current advances in TiO_2-based nanostructure electrodes for high performance lithium ion batteries. Batteries. 2018; 4: 7.
53. Nachit W, Touhtouh S, Ramzi Z, Benkhouja K, Yazami R. TiO_2 nanoparticles prepared by sol-gel method for anode application in lithium-ion batteries. In: Lithium-ion batteries-thin film for energy materials and devices. London: IntechOpen; 2019. pp.93.
54. Liu Y, Yang Y. Recent progress of TiO_2-based anodes for Li ion batteries. J Nanomater. 2016; 4: 8123652.
55. Guler MO, Cevher O, Cetinkaya T, Tocoglu U, Akbulut H. High capacity TiO_2 anode materials for Li-ion batteries. Energy Convers Manag. 2013; 72: 111-116.
56. Lu B, Ma B, Deng X, Wu B, Wu Z, Luo J, Wang X, et al. Dual stabilized architecture of hollow Si@TiO_2@C nanospheres as anode of high-performance Li-ion battery. Chem Eng J. 2018; 351: 269-279.

Enjoy *JEPT* by:

1. Submitting a manuscript
2. Joining in volunteer reviewer bank
3. Joining Editorial Board
4. Guest editing a special issue

For more details, please visit:
http://www.lidsen.com/journal/jept